Deep-to-shallow level transition of Re and Nb dopants in monolayer MoS$_2$ with dielectric environments

Ji-Young Noh,[1,2] Hanchul Kim,[2] Minkyu Park,[3] and Yong-Sung Kim[1,3,*]

[1]*Korea Research Institute of Standards and Science, Yuseong, Daejeon 305-340, Korea*
[2]*Department of Nano Physics, Sookmyung Women's University, Seoul 140-742, Korea*
[3]*Department of Nano Science, University of Science and Technology, Daejeon 305-350, Korea*

We investigate the effects of dielectric environments on the transition levels of Re and Nb dopants in monolayer MoS$_2$ through density functional theory calculations. The inherently weakly screened Coulomb interaction in free-standing monolayer MoS$_2$ makes the dopant electrons and holes strongly bound, and the Re and Nb impurities are found to produce deep levels. It is shown that when the monolayer MoS$_2$ is placed near high permittivity dielectrics the screened Coulomb interaction induces carrier delocalization with generating shallow levels.

PACS number(s): 73.20.Hb, 73.20.Jc, 73.22.Dj, 71.55.Ht

Low-dimensional semiconductors have unique properties that are not present in conventional bulk semiconductors. In a free-standing low-dimensional semiconductor, Coulomb interactions between charges are generally weakly screened, and as consequences (i) large quasiparticle renormalization energy (electron-electron) [1–6], (ii) large exciton binding energy (electron-hole) [1–6], (iii) a large scattering cross section of carriers by charged defects (carrier-electron–charged-defect) [7–9], (iv) deep levels of defects (bound-electron–charged-defect) [10], and (v) large electrostatic interaction energy between charged defects (charged-defect–charged-defect) [10] are induced as their typical features.

The strong Coulomb interactions can be effectively screened by dielectric environments surrounding the low-dimensional semiconductor, and the dielectric screening effect can make great changes in the material's (intrinsic) properties. Atomically thin transition-metal dichalcogenides (TMDs) [11] are novel two-dimensional (2D) semiconductors, which have attracted tremendous interest recently. While the band gap of a free-standing monolayer (ML) MoSe$_2$ is 2.26 eV, it reduces down to 2.13 eV with a bilayer graphene substrate [1]. The exciton binding energy of a free-standing ML-MoSe$_2$ is 0.65 eV, but it weakens to 0.52 eV with a bilayer graphene substrate [1]. Not only with a substrate, additionally with a dielectric encapsulation, the property changes by the environments are even more remarkable. The carrier mobility of electrons of a ML-MoS$_2$ is ~ 1 cm^2 V^{-1} s^{-1} in a ML-MoS$_2$/SiO$_2$ stacked bottom gate thin-film transistor (TFT) [12], while it increases to ~ 200 cm^2 V^{-1} s^{-1} in a HfO$_2$/ML-MoS$_2$/SiO$_2$ stacked top gate structure [13,14]. As such, for the low-dimensional semiconductors, the material's properties depend on where the material is.

Shallow level defects are enormously important in semiconductors to control the electrical conductivity, and efficient n- and p-type doping technologies are essential prerequisites for electronic device applications. However, especially in low-dimensional semiconductors, generation of a shallow level is not always a simple job, because the defect electrons are typically localized near the defect center through the strong bound-

electron–charged-defect Coulomb interaction. In 2D TMDs, the situation is not expected to be different. Nonetheless, the ML-MoS$_2$ has shown a good n-type conductivity, which is unintentionally doped [15,16], and the n-type ML-MoS$_2$ TFTs have been successfully fabricated [13,14]. Recently, Re and Nb [17] impurities are suggested as possible shallow level dopants in free-standing ML-MoS$_2$, through investigating the Kohn-Sham (KS) levels in density functional theory (DFT) calculations [18,19]. However, the strong electron-electron interaction in free-standing ML-MoS$_2$ makes it doubted whether such an independent particle picture provides correct defect transition levels qualitatively as well as quantitatively. Charging with electron inclusion in or electron exclusion out of the system always results in electronic relaxation of the total system of electrons by the electron-electron interactions. When we study a charged state of a defect with the rigid bands or density of states obtained from a neutral defect, this electronic relaxation effect is neglected. The delta self-consistent field (SCF) approach [20] uses the DFT total energies of the charged as well as neutral defects to determine the electronic transition levels of defects, and the electronic relaxation with the charging is included within the DFT level. Since the low-dimensional semiconductors are always under some environments in isolated as well as in integrated devices, understanding the environment dependence of their properties is of big importance.

In this work, we investigate the defect transition levels of Re and Nb impurities in ML-MoS$_2$ using the delta SCF approach based on DFT calculations. It is shown that the Re and Nb impurities are deep level defects in free-standing ML-MoS$_2$. The ML-MoS$_2$ is placed on a (SiO$_2$ or HfO$_2$) substrate and/or below an (SiO$_2$ or HfO$_2$) encapsulation, and the defect transition levels are found to shoal with increasing the environmental dielectric constants. The screened Coulomb interaction between the bound electron and the charged impurity induces the deep-to-shallow level transition in ML-MoS$_2$ with the dielectric environments.

We performed DFT calculations as implemented in the Vienna *ab initio* simulation package (VASP) code [21,22]. The ultrasoft pseudopotentials [23] and the local density approximation (LDA) [24] were used. A kinetic-energy cutoff of 350 eV and $2 \times 2 \times 1$ Γ-centered k-point mesh in 6×6 ML-MoS$_2$ supercells were used. For comparison, the defects
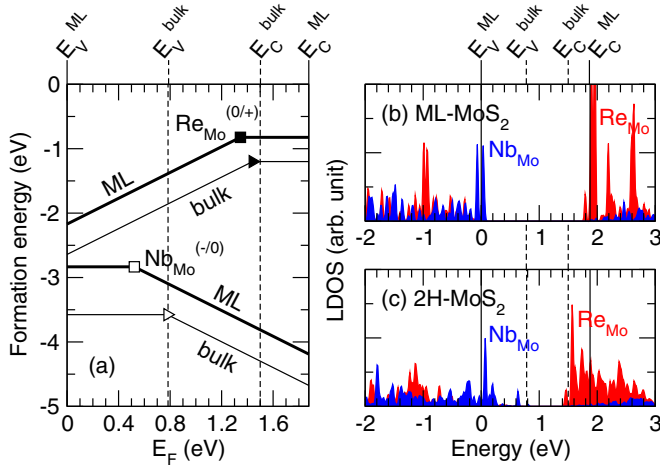
*yongsung.kim@kriss.re.kr

FIG. 1. (Color online) (a) Calculated formation energies of Re_{Mo} and Nb_{Mo} in the neutral and singly charged states of the supercells in free-standing ML-MoS_2 (thick solid lines) and bulk 2H-MoS_2 (thin solid lines) as a function of the Fermi level (E_F). The $Re_{Mo}^{(0/+)}$ donor and $Nb_{Mo}^{(-/0)}$ acceptor transition levels are indicated by the filled and open symbols, respectively. The square symbols are for the dopants in free-standing ML-MoS_2, and the triangle symbols are for those in bulk 2H-MoS_2. Local electronic densities of states of Re_{Mo} (red) and Nb_{Mo} (blue) in (b) free-standing ML-MoS_2 and (c) bulk 2H-MoS_2 are shown. The band edges of bulk 2H-MoS_2 are indicated by vertical dashed lines.

in bulk 2H-MoS_2 were computed with a $6\times6\times3$ supercell and $2 \times 2 \times 2$ Γ-centered k-point mesh. For charged defects, the spurious electrostatic interaction between supercells was eliminated using the model charge correction scheme [10,25–29]. Inclusion of van der Waals interaction with the DFT-D2 scheme [30] did not alter our results.

Figure 1(a) shows the calculated formation energies of the Mo-substitutional Re (Re_{Mo}) and Nb (Nb_{Mo}) defects in bulk 2H-MoS_2 and free-standing ML-MoS_2, as a function of the Fermi level (E_F). The reference systems for the element reservoirs are the hcp Re, bcc Nb, orthorhombic S, and pristine 2H-MoS_2 for the bulk case and pristine free-standing ML-MoS_2 for the ML case. This is the S-rich limit condition in MoS_2. The zero of E_F is set to the valence-band maximum (VBM) of the pristine free-standing ML-MoS_2 (E_V^{ML}), and the upper bound is set to its conduction-band minimum (CBM) (E_C^{ML}), both of which are located at the K valley in the 1×1 Brillouin zone. The VBM of the bulk 2H-MoS_2 (E_V^{bulk}) (located at the Γ valley) is about 0.8 eV above the E_V^{ML}, and the CBM of the bulk 2H-MoS_2 (E_C^{bulk}) (located at a point in the Σ line) is about 0.4 eV below the E_C^{ML}. The band-edge levels of the bulk 2H-MoS_2 are indicated by the vertical dashed lines in Fig. 1(a).

The Re_{Mo} and Nb_{Mo} defects are found to have negative formation energies in the S-rich limit condition. In n-type MoS_2, the formation energy of Re_{Mo} is -1.2 eV in bulk 2H-MoS_2 (when $E_F = E_C^{bulk}$) and -0.8 eV in free-standing ML-MoS_2 (when $E_F = E_C^{ML}$). In p-type MoS_2, the formation energy of Nb_{Mo} is -3.6 eV in bulk 2H-MoS_2 (when $E_F = E_V^{bulk}$) and -2.8 eV in free-standing ML-MoS_2 (when $E_F = E_V^{ML}$). These indicate that the incorporation of Re and Nb

impurities in S-rich bulk 2H- and free-standing ML-MoS_2 is energetically favorable. The Re_{Mo} is a donorlike and Nb_{Mo} is an acceptorlike defect. Figure 1(b) shows the local densities of KS levels for the Re_{Mo} and Nb_{Mo} defects in free-standing ML-MoS_2, and Fig. 1(c) shows those in bulk 2H-MoS_2, in the neutral charge state of the supercells. The KS impurity levels of the Re_{Mo} and Nb_{Mo} are found to be near E_C^{ML} and E_V^{ML}, respectively, in free-standing ML-MoS_2 [Fig. 1(b)], as previously shown in a DFT study [18], and they are just above and well below the E_C^{bulk} and E_V^{bulk} levels, respectively, in bulk 2H-MoS_2 [Fig. 1(c)].

The Re_{Mo}^{1+} and Nb_{Mo}^{1-} formation energies are calculated based on the delta SCF DFT approach, and the $Re_{Mo}^{(0/+)}$ donor and $Nb_{Mo}^{(-/0)}$ acceptor transition levels are estimated. In free-standing ML-MoS_2, the calculated $Re_{Mo}^{(0/+)}$ and $Nb_{Mo}^{(-/0)}$ defect levels are $E_C^{ML} - 0.53$ eV and $E_V^{ML} + 0.52$ eV, respectively, as shown in Fig. 1(a). This means that when $E_F = E_C^{ML}$ the Re_{Mo}^0 is the most stable and the electronic excitation of $Re_{Mo}^0 \rightarrow Re_{Mo}^{1+} + e^-$ requires 0.53 eV, where e^- is a conduction electron. When $E_F = E_V^{ML}$, the Nb_{Mo}^0 is the most stable and the excitation of $Nb_{Mo}^0 \rightarrow Nb_{Mo}^{1-} + h^+$ requires 0.52 eV, where h^+ is a valence hole. The electronic relaxation with adding or removing an electron from the impurity center is important, and as expected from the strong electron-electron Coulomb interaction the KS levels within the LDA [Fig. 1(b)] fail to describe the deep nature of the Re_{Mo} and Nb_{Mo} defects in free-standing ML-MoS_2.

On the other hand, in bulk 2H-MoS_2, the Re_{Mo} and Nb_{Mo} defects generate shallow levels. The calculated $Re_{Mo}^{(0/+)}$ donor level is $E_C^{bulk} - 0.06$ eV (at best qualitative) in bulk 2H-MoS_2, as shown in Fig. 1(a). The formation energies of Nb_{Mo} in the neutral and ($1-$) charged states of the supercell cross near E_V^{bulk} [see the open triangle in Fig. 1(a)]. Since the Nb_{Mo} defect KS level is well inside the bulk valence bands [Fig. 1(c)], the doped hole occupies the band-edge state E_V^{bulk}, when $E_F = E_V^{bulk}$, and the neutral charge state of the Nb_{Mo}-containing supercell actually means $Nb_{Mo}^{1-} + h^+$. The shallow nature of the Re_{Mo} and Nb_{Mo} defects in bulk 2H-MoS_2 originates in part from the band-edge shifts from the ML ones, as indicated by the E_C^{ML} and E_C^{bulk}, and E_V^{ML} and E_V^{bulk} in Fig. 1(a). If we compare the $Re_{Mo}^{(0/+)}$ donor levels in bulk and free-standing ML-MoS_2 from the E_C^{ML}, it is closer to E_C^{ML} in bulk 2H-MoS_2 than in free-standing ML-MoS_2 [see the filled triangle at the right side of the filled square in Fig 1(a)]. This implies that the bound-electron–charged-impurity Coulomb interaction weakens more in bulk 2H-MoS_2 than in free-standing ML-MoS_2, as a result of the dielectric screening from the environment (the other MoS_2 layers) surrounding the Re_{Mo}-containing MoS_2 layer in bulk 2H-MoS_2.

We consider various dielectric environments surrounding a ML-MoS_2. Figures 2(a)–2(f) show the model atomic structures for the free-standing ML-MoS_2: vacuum/MoS_2/vacuum (VMV), vacuum/MoS_2/SiO_2 (VMS), SiO_2/MoS_2/SiO_2 (SMS), vacuum/MoS_2/HfO_2 (VMH), HfO_2/MoS_2/SiO_2 (HMS), and HfO_2/MoS_2/HfO_2 (HMH) systems. The in-plane periodicity of the ML-MoS_2 is 6×6. The SiO_2 is modeled by 4×4 α-quartz $SiO_2(0001)$ slab, on which the surface dangling bonds are passivated by H, and the HfO_2 is modeled
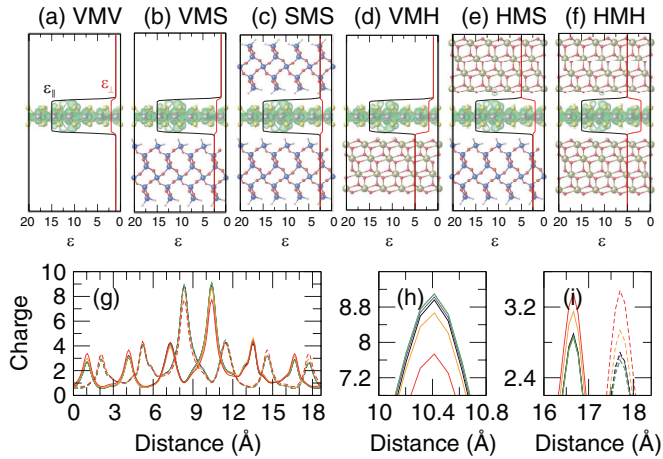
FIG. 2. (Color online) Atomic structures of the (a) VMV, (b) VMS, (c) SMS, (d) VMH, (e) HMS, and (f) HMH model systems. The structures include Mo (purple), S (yellow), Si (blue), Hf (gold), O (red), and H (white) atoms. The dielectric constant real-space profiles across the slabs and the charge isosurfaces of the Re_{Mo} defect states are shown in (a)–(f). (g)–(i) Plane-averaged Re_{Mo} defect charge densities in VMV (black), VMS (purple), SMS (blue), VMH (green), HMS (orange), and HMH (red) along the in-plane lattice vector directions (solid and dashed lines). (g), (h) Magnification of the area near the impurity center. (i) Magnification of the area far from the impurity center.

FIG. 3. (Color online) (a) Calculated formation energies of Re_{Mo} and Nb_{Mo} defects in the neutral and singly charged states in VMV (black), VMS (purple), SMS (blue), VMH (green), HMS (orange), and HMH (red) as a function of the Fermi level (E_F) with respect to E_V^{ML}. Those as a function of E_F with respect to E_V^{XMX} are plotted in the inset of (a). The $Re_{Mo}^{(0/+)}$ donor and $Nb_{Mo}^{(-/0)}$ acceptor transition levels are indicated by the filled and open symbols, respectively. (b) The donor and acceptor transition levels as a function of the environmental dielectric constant ε_E.

by an O-terminated 5×5 cubic $HfO_2(111)$ slab. The SiO_2 and HfO_2 are strained by $+1.1$ and $+6.0\%$, respectively, to match their lattice constants to that of the ML-MoS_2 (3.124 Å in LDA for the free-standing ML-MoS_2). Six (five) Si or four (four) Hf atomic layers are used for the bottom (top) dielectric slab. The interface spacing between the MoS_2 and SiO_2 (HfO_2) is 2.45 (2.74) Å. The Re_{Mo} and Nb_{Mo} defects, separately, are put into the ML-MoS_2 that has the nearby dielectrics, and the formation energies and defect transition levels are calculated. The Hellmann-Feynman forces are relaxed only for the free-standing ML-MoS_2 with Re_{Mo} and Nb_{Mo} until less than 0.01 eV/Å, and it is used for the Re_{Mo}- and Nb_{Mo}-doped ML-MoS_2 with the dielectric environments (no further atomic relaxations). The atomic structures of the SiO_2 and HfO_2 dielectrics are not relaxed. A test for the VMS system including the atomic relaxation shows no essential change in the results.

Figure 3(a) shows the calculated DFT formation energies of the neutral and ionized Re_{Mo} and Nb_{Mo} in the ML-MoS_2 with the dielectric environments, as a function of E_F. The zero of E_F is set to the E_V^{ML} of the pristine free-standing ML-MoS_2 (VMV), and the upper bound (1.877 eV) of the E_F is the E_C^{ML} of the pristine free-standing ML-MoS_2. With the dielectric environments, the CBMs of the pristine ML-MoS_2 (E_C^{XMX}, where $X = V$, S, or H) are found to be nearly the same as that of the pristine free-standing ML-MoS_2 (E_C^{ML}), while the shifts of the VBMs of the pristine ML-MoS_2 with the HfO_2 dielectrics (E_V^{XMH}, where $X = V$, S, or H) from the E_V^{ML} are not negligible. (The S-$3p$ contribution is larger in the E_V^{ML} state at the Γ point than in the E_C^{ML} state, and the interface hybridization is stronger in the E_V^{ML} state.) The VBM shifts with SiO_2 dielectrics are small [16]. The E_V^{XMX}'s are indicated
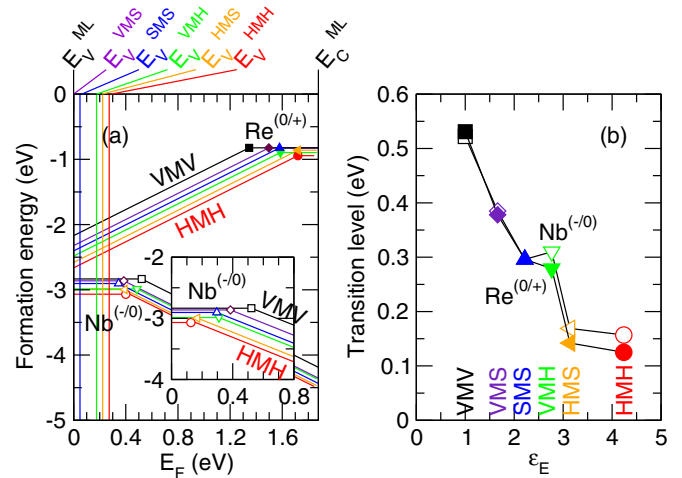
by the vertical lines near $E_F = 0.0$–0.3 eV in Fig. 3(a). Setting the zero of E_F to the E_V^{XMX}'s of the pristine ML-MoS_2's with the dielectrics, the formation energies of the Nb_{Mo} are plotted in the inset of Fig. 3(a). The transition levels of the $Re_{Mo}^{(0/+)}$ and $Nb_{Mo}^{(-/0)}$ are found to be shallower, close to the CBMs and VBMs, respectively, of the ML-MoS_2's with the dielectrics, in order of the VMV, VMS, SMS, VMH, HMS, and HMH structures for $Re_{Mo}^{(0/+)}$ and in order of the VMV, VMS, VMH, SMS, HMS, and HMH for $Nb_{Mo}^{(-/0)}$.

The electronic contributions of the dielectric constants of bulk SiO_2 and HfO_2 are calculated to be 2.5 and 5.0, respectively, using density functional perturbation theory [31] in LDA level. That of the free-standing ML-MoS_2 is calculated to be 15 (in plane) and 2 (out of plane), and we plot the dielectric constant (real-space) profiles across the slabs in Figs. 2(a)–2(f). We define the environmental dielectric constant (ε_E) as $\varepsilon_E = (\varepsilon_T t_T + t_C + \varepsilon_B t_B)/L_z$, where the ε_T and ε_B are the dielectric constants of the top and bottom dielectrics, respectively; the t_T and t_B are the thicknesses of the top and bottom dielectrics, respectively; t_C is the thickness of the ML-MoS_2; and the L_z is the length of the supercell normal to the layers ($t_T = 11.741$ Å, $t_C = 6.033$ Å, $t_B = 14.060$ Å, and $L_z = 31.834$ Å). The calculated ε_E's are 1.000 (VMV), 1.662 (VMS), 2.216 (SMS), 2.767 (VMH), 3.138 (HMS), and 4.242 (HMH). The transition levels of the $Re_{Mo}^{(0/+)}$ and $Nb_{Mo}^{(-/0)}$ are plotted as a function of ε_E in Fig. 3(b), showing that the Re_{Mo} donor and Nb_{Mo} acceptor transition levels nearly monotonically decrease with ε_E.

The charge densities of the Re_{Mo} (representatively) defect state in ML-MoS_2 with the dielectric environments are compared in Fig. 2. The charge isosurfaces are shown in Figs. 2(a)–2(f), and the plane-averaged charge densities are

shown in Figs. 2(g)–2(i) along the in-plane lattice vector directions (solid and dashed lines). The spatial distributions of the defect charge densities are found to be delocalized with the dielectric environments. Those in the central region where the impurity is located are reduced [Fig. 2(h)], while those far from the impurity center are increased [Fig. 2(i)], as ε_E increases. The environmental dielectrics near the ML-MoS$_2$ are likely to screen the bound-electron–charged-defect Coulomb interaction in the ML-MoS$_2$ and make the defect charge density spread out, resulting in the shallow levels.

In conclusion, the Mo-substitutional Re and Nb impurities in free-standing ML-MoS$_2$ are deep level defects, while they are shallow level ones in bulk 2H-MoS$_2$. When the ML-MoS$_2$ is placed with nearby other materials (as in a device structure), the Re$_{Mo}$ and Nb$_{Mo}$ defect states are found to be shallower. The intrinsic Coulomb interaction in free-standing ML-MoS$_2$ is strong, but it can be effectively screened by dielectric environments surrounding the ML-MoS$_2$. With a HfO$_2$ encapsulation, the Re$_{Mo}$ and Nb$_{Mo}$ are found to be a shallow donor and acceptor, respectively, in ML-MoS$_2$ on a SiO$_2$ or HfO$_2$ substrate, of which structure and dopants can be utilized in ML-MoS$_2$-based electronic devices.

[1] M. M. Ugeda, A. J. Bradley, S.-F. Shi, F. H. da Jornada, Y. Zhang, D. Y. Qiu, W. Ruan, S.-K. Mo, Z. Hussain, Z.-X. Shen, F. Wang, S. G. Louie, and M. F. Crommie, Nat. Mater. **13**, 1091 (2014).

[2] T. Cheiwchanchamnangij and W. R. L. Lambrecht, Phys. Rev. B **85**, 205302 (2012).

[3] A. Ramasubramaniam, Phys. Rev. B **86**, 115409 (2012).

[4] H. P. Komsa and A. V. Krasheninnikov, Phys. Rev. B **86**, 241201 (2012).

[5] H. Shi, H. Pan, Y.-W. Zhang, and B. I. Yakobson, Phys. Rev. B **87**, 155304 (2013).

[6] D. Y. Qiu, F. H. da Jornada, and S. G. Louie, Phys. Rev. Lett. **111**, 216805 (2013).

[7] D. Jena and A. Konar, Phys. Rev. Lett. **98**, 136805 (2007).

[8] N. Ma and D. Jena, Phys. Rev. X **4**, 011043 (2014).

[9] W. Bao, X. Cai, D. Kim, K. Sridhara, and M. S. Fuhrer, Appl. Phys. Lett. **102**, 042104 (2013).

[10] J.-Y. Noh, H. Kim, and Y.-S. Kim, Phys. Rev. B **89**, 205417 (2014).

[11] Q. H. Wang, K. Kalantar-Zadeh, A. Kis, J. N. Coleman, and M. S. Strano, Nat. Nanotechnol. **7**, 699 (2012).

[12] K. S. Novoselov, D. Jiang, F. Schedin, T. J. Booth, V. V. Khotkevich, S. V. Morozov, and A. K. Geim, Proc. Natl. Acad. Sci. USA **102**, 10451 (2005).

[13] B. Radisavljevic, A. Radenovic, J. Brivio, V. Giacometti, and A. Kis, Nat. Nanotechnol. **6**, 147 (2011).

[14] B. Radisavljevic and A. Kis, Nat. Mater. **12**, 815 (2013).

[15] H. Fang, M. Tosun, G. Seol, T. C. Chang, K. Takei, J. Guo, and A. Javey, Nano Lett. **13**, 1991 (2013).

[16] K. Dolui, I. Rungger, and S. Sanvito, Phys. Rev. B **87**, 165402 (2013).

[17] M. R. Laskar, D. N. Nath, L. Ma, E. W. Lee II, C. H. Lee, T. Kent, Z. Yang, R. Mishra, M. A. Roldan, J.-C. Idrobo, S. T. Pantelides, S. J. Pennycook, R. C. Myers, Y. Wu, and S. Rajan, Appl. Phys. Lett. **104**, 092104 (2014).

[18] K. Dolui, I. Rungger, C. Das Pemmaraju, and S. Sanvito, Phys. Rev. B **88**, 075420 (2013).

[19] Y.-C. Lin, D. O. Dumcenco, H.-P. Komsa, Y. Niimi, A. V. Krasheninnikov, Y.-S. Huang, and K. Suenaga, Adv. Mater. **26**, 2857 (2014).

[20] G. Onida, L. Reining, and A. Rubio, Rev. Mod. Phys. **74**, 601 (2002).

[21] G. Kresse and J. Furthmüller, Comput. Mater. Sci. **6**, 15 (1996).

[22] G. Kresse and J. Furthmüller, Phys. Rev. B **54**, 11169 (1996).

[23] D. Vanderbilt, Phys. Rev. B **41**, 7892 (1990).

[24] D. M. Ceperley and B. J. Alder, Phys. Rev. Lett. **45**, 566 (1980).

[25] C. Freysoldt, J. Neugebauer, and C. G. Van de Walle, Phys. Rev. Lett. **102**, 016402 (2009).

[26] H.-P. Komsa, T. T. Rantala, and A. Pasquarello, Phys. Rev. B **86**, 045112 (2012).

[27] H.-P. Komsa and A. Pasquarello, Phys. Rev. Lett. **110**, 095505 (2013).

[28] Y. Kumagai and F. Oba, Phys. Rev. B **89**, 195205 (2014).

[29] H.-P. Komsa, N. Berseneva, A. V. Krasheninnikov, and R. M. Nieminen, Phys. Rev. X **4**, 031044 (2014).

[30] S. Grimme, J. Comp. Chem. **27**, 1787 (2006).

[31] S. Baroni and R. Resta, Phys. Rev. B **33**, 7017 (1986).